Novel improvised satin bowerbird algorithm for speed control and torque ripple minimization for switched reluctance motor

M. Upanya, S. Rashmi
Department of Electrical and Electronics Engineering, Vidyavardhaka College of Engineering, Mysuru, India,
affiliated with Visvesvaraya Technological University, Belagavi, India

Article Info

Article history:

Received Apr 25, 2026
Revised Jul 17, 2026
Accepted Aug 14, 2026

Keywords:

Satin bowerbird algorithm
Speed control
Switched reluctance motor
Torque ripple
Torque sharing function

ABSTRACT

Switched reluctance motors (SRMs) have gained a lot of popularity for adjustable speed drive systems, cost-effectiveness, and simplicity. Currently, SRMs are widely used in electric vehicles, compressors, and machine tools. In the proposed work, the satin bowerbird (SBB) algorithm is improvised and implemented to determine the optimal turn-off angle (θ_{off}), along with gain parameters for the proportional integral (PI) controller, to regulate the speed and to enhance the torque profile of the SRM. The performance of the SRM drive is tested for 4 different control schemes with different load torque and reference speed. The control schemes are a PI controller with hysteresis current control (HCC), implemented with conventional SBB and improvised SBB (ISBB). The other control scheme is a PI controller with an improved torque sharing function (TSF) and HCC, implemented with conventional SBB and improvised SBB. The TSF used in the control scheme has been improvised with adaptive smoothing and adaptive boosting functions. For the different control schemes tested, ISBB with a PI controller and improvised TSF with HCC has resulted in better speed regulation and a 50% reduction in total harmonic distortion (THD) when compared to the control scheme constituting the conventional SBB algorithm with a PI controller and HCC. The proposed work is extended with the computation of torque rising time (T_r) and torque settling time (T_S).

Corresponding Author:

M. Upanya
Department of Electrical and Electronics Engineering, Vidyavardhaka College of Engineering
Mysuru, India
affiliated with Visvesvaraya Technological University
Belagavi, India
Email: upanya.m@vvce.ac.in

1. INTRODUCTION

Switched reluctance motors (SRMs) are gaining more attention in current motor drive applications. The reason being these motors do not make use of permanent magnets. Permanent magnet synchronous motors are widely used for electric and hybrid electric vehicle applications, and these motors provide higher power density, but with respect to the constructional aspect, permanent magnets are required, which demands rare earth metals. SRMs have the advantage of adjustable speed drive [1]. SRMs have the inherent capability to adapt to variable speed [2]. When the performance of SRMs is compared with that of permanent magnet motors for a common switching frequency, SRMs produce less switching loss compared to permanent magnet motors [3]. SRMs have gained scientific popularity due to numerous advantages, as they produce better efficiency when compared to induction motors for the same rating [4]. As there is advancement in the field of power switching devices, SRMs have become suitable for many motor drive applications [5].

Since SRMs are gaining a lot of popularity, there is a need to improve speed control, torque ripple minimization, and efficiency [6]. The challenges in SRMs are high torque ripples, acoustic noise production, and nonlinear behavior [7]-[9]. The proposed work focuses on improving the speed profile and current profile. Improving the current profile improves the torque profile as well. Improving the speed profile of the SRM enhances its application in various directions. The speed control of SRM is achieved by many adaptive controllers through which the effectiveness of the SRM can be demonstrated [10]. Commonly used controllers for SRM are PI controllers. The proportional integral derivative (PID) controller is effective in mitigating ripples of torque, provides dynamic response to disturbance, and ensures accurate motor speed control [11]. A PI-tuned converter can provide more power density, better proficiency, and a smaller motor drive structure [12].

The major aspect that contributes to enhancing the speed and torque profile of SRM is the turn-on and turn-off angles. Appropriate turn-on and turn-off angles combined with the controller enhance the performance of the SRM. Implementation of metaheuristic algorithms to determine the turn-on and turn-off angles helps in aligning the rotor and stator position of the SRM; the right alignment improves the current profile, therefore enhancing the torque profile of the SRM. Metaheuristic techniques such as satin bowerbird (SBB) have gained importance recently; mainly, its chaotic selection aspect provides benefit in enhancing the performance of the system [13]. Metaheuristic algorithms such as particle swarm optimization (PSO) have been implemented along with a PI controller to enhance the speed regulation of SRM [14]. Computation of optimal parameters can be obtained by the implementation of genetic algorithm (GA) [15], whale optimization algorithm (WOA) [16], gravitational search optimization (GSO) [17], and ant colony optimization (ACO) [18]. Grey wolf optimization mimics the leadership, hierarchy, and social dynamics of real grey wolves. The aspects of hunting, prey search and prey encircle and prey attacking can be implemented to determine the optimal parameters of the SRM [19].

This sets the platform for the research to integrate three metaheuristic algorithms along with the controller. The inherent nature of SRMs makes achieving the best performance with these nonlinear characteristics a challenge. Choosing the metaheuristic algorithm to determine the best switching angle enhances the overall performance of the machine [20]. Optimized conduction angle with control strategy expands the operating region and overall performance of the machine [21]. An adaptive turn-on angle function along with a control strategy improves the overall efficiency of the SRM, along with the ability to adapt to changes in speed and load torque [22]. Traditional controllers are used to achieve the rated or reference speed; using a metaheuristic algorithm gives a better dimension to this objective [23].

The heart of SRM operation is energizing the stator poles, which creates magnetic flux; the flux pulls the nearest unmagnetized rotor pole. Energizing the stator poles paves the way for the implementation of a power electronic converter. For an SRM drive, the power converter, which performs DC-DC conversion, plays an important role in providing unipolar current for each winding [24]. The other important nonlinear aspect of SRM is the torque profile. The inherent nature of torque ripple limits the application of SRM [25]; henceforth, the focus shifts to improving the torque profile and better speed regulation of the SRM. In consideration of the literature, improvement in the speed profile, current profile, and torque profile with the implementation of a metaheuristic technique sets the stage for a research hotspot in SRM.

The proposed work aims to develop an improvised torque sharing function (TSF) to improve the torque profile, enabling the SRM for expanded application. The heart of the proposed work is the improvised SBB (ISBB) metaheuristic technique to compute the multi-objective parameters, namely, torque ripple, THD, and speed error. ISBB is implemented to determine the θ_{on}, θ_{off}, and controller gains for PI to compute the multiobjective function at different load torque and speed conditions.

This proposed work aims to develop an ISBB algorithm to determine the θ_{off}, gain parameters of PI controller for speed regulation and torque ripple minimization for SRM, along with determining the torque rising time (T_r) and torque settling time (T_s). The design methodology is presented for 4 different control strategies, namely the SBB with PI controller and hysteresis current control (HCC), ISBB with PI controller and HCC, SBB with PI, TSF and HCC, ISBB with PI, TSF and HCC.

2. METHODOLOGY

6/4 SRM is considered for the proposed work. SRM works on the principle of variable reluctance; the rotor poles try constantly to align in the lowest reluctance path. For an SRM, θ_{on}, and θ_{off} angles are basically the rotor positions for which phase windings get energized or de-energized, respectively. The θ_{on} is basically where the current starts to flow in the phase winding and θ_{off} is basically where the current is stopped also called the maximum inductance region. As per the 6/4 SRM generic model of MATLAB, based on the magnetization characteristics of the machine, inductance rises between 10° to 45° of the rotor position. For the proposed strategy, θ_{on} is fixed and θ_{off} is computed by the SBB algorithm. The reason for manually setting the θon is so that it lies in the positive dθ/dL region. If the θ_{on} is too early, current starts to develop in the low inductance region, practically leading to copper loss; if the θ_{on} is chosen too late leads to insufficient torque development. Hence, to avoid the above-mentioned two conditions, θ_{on} is set manually, and θ_{off} is computed through the algorithm. The following equations are used to calculate the parameters of the SRM. The equivalent voltage of SRM per phase is given in (1).

$$v_{dc} = R_s i + L\frac{d(\lambda,\theta)}{dt} \tag{1}$$

v_{dc} is the terminal voltage, R_s is the resistance, λ is the flux linkage, L is the inductance, and θ is the rotor position. The torque equation for SRM is given in (2).

$$T_e = \frac{1}{2}i^2\frac{dl(\theta)}{d\theta} \tag{2}$$

Positive torque occurs when $\frac{dL(\theta)}{d\theta} > 0$, this is the first criterion to compute the θ_{off} using the algorithm. The (3) is used to calculate the electrical angle between the two aligned positions. The equation is given as (3).

$$\theta_c = \frac{360^0}{N_r} \tag{3}$$

N_r is the number of rotor poles, hence $\theta_c = 90°$ for $N_r = 4$, since it is a 6/4 SRM. With this calculation $\theta_{aligned}$ is 90° this is second criteria to compute the θ_{off} using the algorithm, so current stops before 90°. Current decay is calculated using (4).

$$\frac{di}{dL} = \frac{R_S}{L}i \tag{4}$$

The (5) and (6) is used to compute the rotor speed and current decay with rotor position respectively. Integrating (6) leads to (7).

$$\theta = \omega t \tag{5}$$

$$d(i,\theta) = \frac{R_S}{\omega L}i \tag{6}$$

$$\theta_{off} = \theta_{aligned} - \frac{\omega L}{R_S}ln\frac{i_{peak}}{i_{min}} \tag{7}$$

2.1. Optimization technique: ISBB algorithm

SBB algorithm is based on the life of the satin bowerbird. Attractive bowers are created by the male satin bowerbirds to attract the female satin bowerbirds. SBB algorithms are versatile, and their improved versions are proven to fetch more accurate results [26], [27]. In the proposed work, the conventional SBB is improvised by incorporating chaotic initialization, adaptive exploration, and elite preservation. The stages of the ISBB are as follows.

i) Chaotic initialization: In this phase, the algorithm begins with the formation of an initial set of bowers within the specified search space, where every bower`s position represents a candidate solution. Chaotic population initialization helps in having a uniform distribution for the search space for every bower; diversity of the initial population is maximized and reduces trapping in local minima. Decision vectors are defined as θ_{off}, K_p, and K_i gain values of PI controller. Decision variable bounds are represented as in (8)-(10). Upper bounds (ub) and lower bounds (lb) are initialized for the bower creation. The (11) and (12) are used to compute the initial bowers.

$$\theta_{off}^{min} \leq \theta_{off} \leq \theta_{off}^{max} \tag{8}$$

$$K_p^{min} \leq K_p \leq K_p^{max} \tag{9}$$

$$K_i^{min} \leq K_i \leq K_I^{max} \tag{10}$$

$$Y_{K+1} = 4y_k(1 - y_k) \tag{11}$$

$$Y_i = lb + y_k(ub - lb) \tag{12}$$

ii) Evaluation and adaptive exploration: This is a mate attraction process. In this stage, evaluation of the attractiveness of the bower is carried out by the female birds. This stage supports the adaptability of bowerbirds based on the environmental conditions. The adaptive exploration parameter is mathematically formulated as follows. The (13) represents the evaluation function. The evaluation parameters are e_s the speed error, THD, and torque ripple (R), calculated using (14)-(16), respectively. Adaptive exploration is mathematically formulated as per (17).

$$J = b_1 e_s + b_2 THD + b_3 R \tag{13}$$

$$e_s = \omega_{ref} - \omega \tag{14}$$

$$R = \frac{T_{max} - T_{min}}{T_{avg}} \tag{15}$$

$$THD = \frac{\sqrt{\sum_{k=2}^{N} |Y|_k^2}}{|Y|} \tag{16}$$

$$\sigma = \sigma_0 \left(1 - \frac{iteration}{Maxiteration}\right)^2 \tag{17}$$

iii) Enhanced learning and better social interaction: Since the diversity aspect is considered, bowerbirds compete with multiple individuals and learn as well. This aspect is mathematically formulated as shown in (18).

$$Y_{i_{new}} = y_i + \lambda(y_j - y_k) + \sigma N(0,1) \tag{18}$$

iv) Preservation of the elite: This stage is about preservation of the best or the elite bower. The best solution is preserved in this stage, which is mathematically formulated as per (19).

$$Y_I = \begin{cases} Y_I^{new}, if\ j(Y_i^{new}) < j(Y_i) \\ Y_i,\ ,\ otherwise \end{cases} \tag{19}$$

v) Selection and evolution of bower: In the selection process, it is the selection of the best bower by the female birds. The evolution stage is related to an iteration loop; the process repeats until convergence is met. That is, the process continues till the last iteration value. In this stage, the algorithm will provide the optimal values of θ_{off}, K_p, and K_i.

2.2. Control scheme 1: PI controller with HCC

PI controller is implemented to control the speed of the SRM and reduce the transient response of the system [28]. PI controllers, when tuned with algorithms, produce better results when compared to a conventional PI controller [29]. Integral performance criteria of the PI controller can be improved by using an algorithm [30]. Selecting the adaptive gain values for the PI controller is required for quickly adjusting to varying load conditions [31]. The (20) represents the speed control for the PI controller.

$$Output(t) = K_p e(t) + K_i \int_0^t e(t) d(t) \tag{20}$$

Figure 1 represents the block diagram of control scheme 1 for SRM drive. The components of the SRM drive are as follows. In the H-bridge converter, 6 MOSFETs along with those six diodes are implemented for the control of a 6/4 SRM. Since it is a 6/4 SRM, there are three phases, namely phase A, phase B, phase C. The designated switches and diodes for phase A are S1, S2, D1, D2. Similarly for phase B, S3, S4 and D3, D4, and for phase C, the switches are S5, S6, and D5, D6. Phases are energized in a sequence. If phase A is made to energize, the other two phases are kept idle; similarly, the same technique is applied when phase B and phase C are energized. The actual rotor position is measured in terms of θ. The actual speed of the rotor is measured and compared with the reference speed; the difference in speed generates an error. The error is given as an input to the current controller; the output of the current controller and the logic designed to energize the phase sequence are used to generate gate switching pulses. This output is fed to an

H-bridge converter, which in turn drives the SRM motor. Commonly used control methods in SRM are asymmetrical half-bridge converters with a hysteresis current controller [32]. HCC is known for its high efficiency [33]. H-bridge converters are widely preferred for their availability in the market; mass production of the converter is available, and replacement in the event of failure is easy [34]. HCC method is widely used for stationary or rotating framework [35].

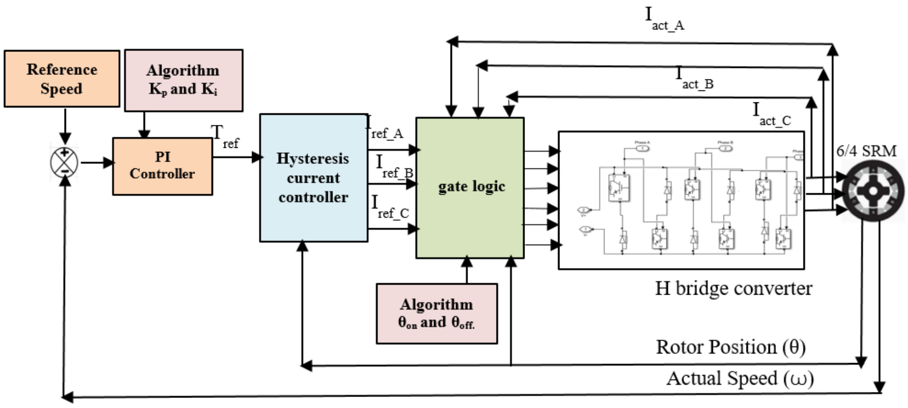

Figure 1. Block diagram of control scheme 1 for SRM drive

2.3. Control scheme 2: PI controller with TSF and HCC

Figure 2 represents the block diagram of control scheme 2, which includes a PI controller, torque sharing function (TSF) block, torque to current converter, hysteresis block combined with gating logic, and H-bridge converter with SRM. TSFs are control techniques implemented to minimize torque ripples in SRMs. Key types include cubic, sinusoidal, exponential, linear, hybrid, and higher-order polynomial functions. For the proposed control scheme, a quintic polynomial is used in TSF, which is a higher-order polynomial function. The advantage of a quintic polynomial is that it offers a higher degree of freedom, allowing for a smooth profile and lower torque ripple. The basic quintic polynomial is represented in (21).

$$f(z) = c_0 + c_1 z^1 + c_2 z^2 + c_3 z^3 + c_4 z^4 + c_5 z^5 \tag{21}$$

This is a fifth-order polynomial, and six conditions are needed to determine it. The six boundary conditions are as follows.

The first two conditions are with respect to torque level. At turn-on, torque being minimum and at full conduction, torque being maximum is represented in (22) and (23), respectively.

$$f(0) = 0 \tag{22}$$

$$f(1) = 1 \tag{23}$$

Substituting (22), the basic quintic polynomial equation is derived as shown in (24).

$$f(0) = 0, C_0 = 0 \tag{24}$$

Substituting (23), the basic quintic polynomial equation is derived as represented in (25).

$$f(1) = 1, c_0 + c_1 + c_2 + c_3 + c_4 + c_5 = 1 \tag{25}$$

For the 3rd and 4th boundary conditions, the first derivative of the quintic polynomial is represented by (26), considered for smooth current operation where the current entry and exit are smooth.

$$f'(z) = \mathrm{c}_1 + 2\mathrm{c}_2 Z + 3\mathrm{c}_3 \mathrm{z}^2 + 4\mathrm{c}_4 \mathrm{z}^3 + 5\mathrm{c}_5 \mathrm{z}^4 \tag{26}$$

With the implementation of the first boundary condition, the coefficient C1 is obtained as per (27).

$$f'(0) = 0,\ C_1 = 0 \tag{27}$$

With the implementation of the second boundary condition, the first derivative (26) and (29) are obtained.

$$f'(1) = 0, \quad (28)$$

$$2c_2 + 3c_3 + 4c_4 + 5c_5 = 0 \quad (29)$$

As a 5th and 6th boundary condition, the second derivative of the quintic polynomial represented in (30) is considered to avoid the sudden rise in acceleration of torque and for a smoother transition of torque.

$$f''(z) = 2c_2 + 6c_3z + 12c_4z^2 + 20c_5z^3 \quad (30)$$

With the implementation of the 1st boundary condition to the second derivative, C2 is obtained as represented in (31). Implementation of secondary condition leads to (32).

$$f''(0) = 0,\ 2c_2 = 0 \quad (31)$$

$$f''(1) = 0,\ \ 6c_3 + 12c_4 + 20c_5 = 0 \quad (32)$$

With C_0=0, C_1=0, C_2=0, the remaining polynomial is represented in (33).

$$f(z) = c_3z^3 + c_4z^4 + c_5z^5 \quad (33)$$

From the function condition, (34) is obtained.

$$c_3 + c_4 + c_5 = 1 \quad (34)$$

Solving the first derivative of (33), (35) is obtained.

$$3c_3 + 4c_4 + 5c_5 = 0 \quad (35)$$

Solving the second derivative of (33), (36) is obtained.

$$6c_3 + 12c_4 + 20c_5 = 0 \quad (36)$$

Solving (35) and (36) simultaneously, values of the coefficients are derived.

$$c_3 = \frac{5}{3}c_5,\ \ c_5 = 6,\ \ \ c_4 = -15, c_3 = 10$$

With the substitution of all the coefficients, the basic quintic polynomial is deduced to (37).

$$f(z) = 10z^3 - 15z^4 + 6z^5 \quad (37)$$

$$z = \frac{\theta - \theta_{on}}{\theta_{off} - \theta_{on}} \quad (38)$$

In the proposed work, algorithm provides the $\theta_{off,}$ quintic polynomial serves as a best choice as it basically works for position based which are basically θ_{on} and $\theta_{off.}$ TSF blocks receive the θ_{on} and θ_{off} from the algorithm; based on the conduction region of the phases, TSF provides the enabling function to the respective torque-to-current controller. The torque-to-current controller blocks receive the reference torque from the PI controller and the enabling function from the TSF block. As per (39) mentioned, torque is converted to current. The raw reference current is not directly used as it causes sudden current transitions, more current ripple, and poor commutation behavior, causing more stress on the converter. Hence, adaptive smoothing is implemented in the torque-to-current converter block along with small adaptive boosting as per the equations, respectively.

$$i_u^* = x(\theta)i_r + \big(1 - x(\theta)\big)pre \quad (39)$$

$$i_r = \sqrt{\frac{2T_e}{\frac{dl}{d\theta}}} \quad (40)$$

$$x(\theta) = r + sf_e(\theta) \quad (41)$$

$$i_u^s = i_u^* + h * f_e(\theta) \quad (42)$$

The (41) and (42) contribute to adaptive smoothing; r and s are the scaling aspects considered for adaptive smoothing. At the beginning and end of commutation, the TSF region will be small, as it is the stage where torque starts to develop; the enabling function will be approximately zero, and there exists only the r scaling aspect, leading to smoother current build-up and stronger filtering, leading to soft commutation. Soft commutation reduces the stress on the converter. During the high TSF region, the enabling function and scaling aspect will be maximum, leading to quicker torque response, faster torque establishment, and adaptive smoothing. During commutation in the SRM, there is a sudden change in inductance causing the current to lag and dip in torque; the boosting term compensates the lag in transients. As per (40), boosting is proportional to TSF; compensation automatically adapts to torque demand. During the low torque region, boosting becomes negligible, avoiding unnecessary current injection. During the high torque region, boosting is maximum, leading to quick torque buildup.

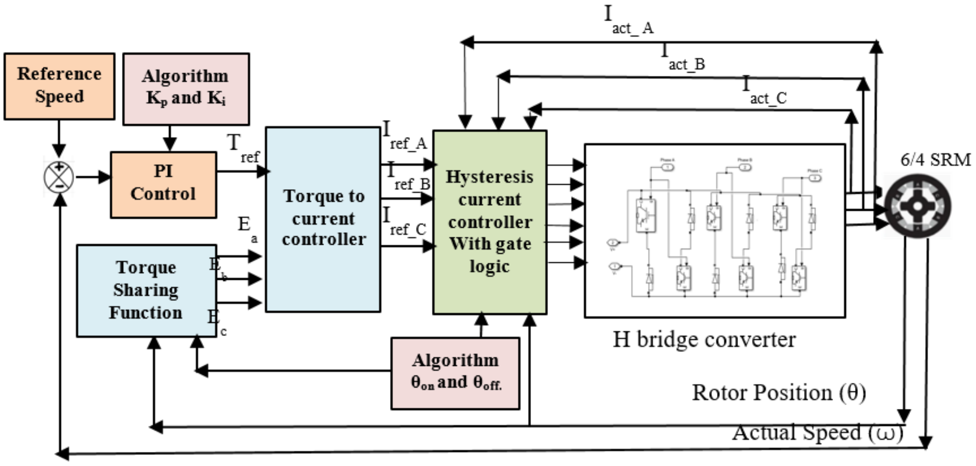

Figure 2. Block diagram of control scheme 2 for SRM drive

3. RESULTS AND DISCUSSION

A simulation model of the 6/4 SRM is built in MATLAB/Simulink to analyze the performance of the SRM with respect to speed and torque ripple minimization for the different control schemes proposed. The different control schemes, along with the algorithm, are implemented for 4 different cases. The SBB and ISBB algorithms compute the θ_{off}, k_p, k_i for the given reference speed and load torque (TL) value. Figure 3 represents the MATLAB/Simulink model of the proposed work. The algorithm is incorporated into the Simulink model to compute the parameters of the controller and θ_{off}, for the given reference speed and load torque. The algorithm is carried out for a population size of 10; the iteration count is 10. To verify the performance, 4 different conditions are considered, namely different rotor speeds (1500 rpm and 1000 rpm) and different load torques (2 Nm and 3 Nm). The ISBB is compared with existing algorithms, namely PSO, GA, WOA, GSO, and ACO.

3.1. Case 1

TL = 2 Nm and reference speed 1500 rpm. Table 1 represents the results of different control strategies for case 1. For the control scheme SBB with PI and HCC, the achieved torque ripple is 1.65, and the speed initially has a small dip at 0.2 s. The control scheme with ISBB, PI, and HCC has achieved a torque ripple of 1.55. In this control scheme, the speed faces a small dip. For the control scheme with SBB, PI, TSF, and HCC, the torque ripple is 1.39. In the ISBB control scheme with PI, TSF, and HCC, the gain parameter values are comparatively less compared to other schemes. The torque ripple is 1.29, and the speed error is less compared to the other 3 schemes. Figure 4(a) represents the speed comparison plot for all the 4 control schemes of case 1. Figure 4(b) represents the torque profile comparison for all the 4 control schemes of case 1. It is very evident that implementation of adaptive TSF has resulted in a better torque profile with less sharp spikes as compared to control schemes with PI and HCC, due to the implementation of adaptive smoothing and adaptive boosting. Figure 4(c) represents the current and flux profile with the PI and HCC control scheme. Figure 4(d) represents the current and flux profile for the control scheme with PI, improvised TSF, and HCC.

The flux and current profile with improvised TSF are more uniform, and the shaping of the current profile has improved as compared to the current and flux profile of the PI and HCC control scheme. Hence, the torque profile is more efficient with the TSF scheme, leading to 50% lower THD. The existing algorithms are compared with ISBB for the proposed TSF. The ISBB strikes the perfect balance in finding the θ_{off}, k_p, and K_i to compute the minimum speed error and THD. The features of ISBB are chaotic initialization, which provides better global search. The existing algorithms work on random initialization, leading to local minima trapping. A differential search mechanism employed with differential learning and Gaussian mutation leads to better search diversity and adaptive exploration. The elite mechanism of ISBB avoids the loss of the best solution.

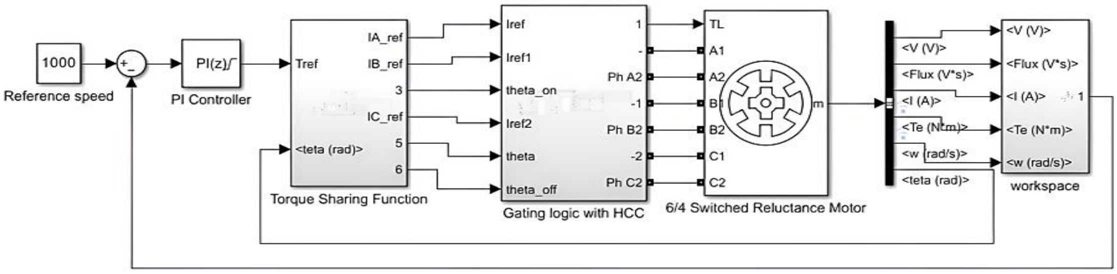

Figure 3. Block diagram of control scheme 2 for SRM drive

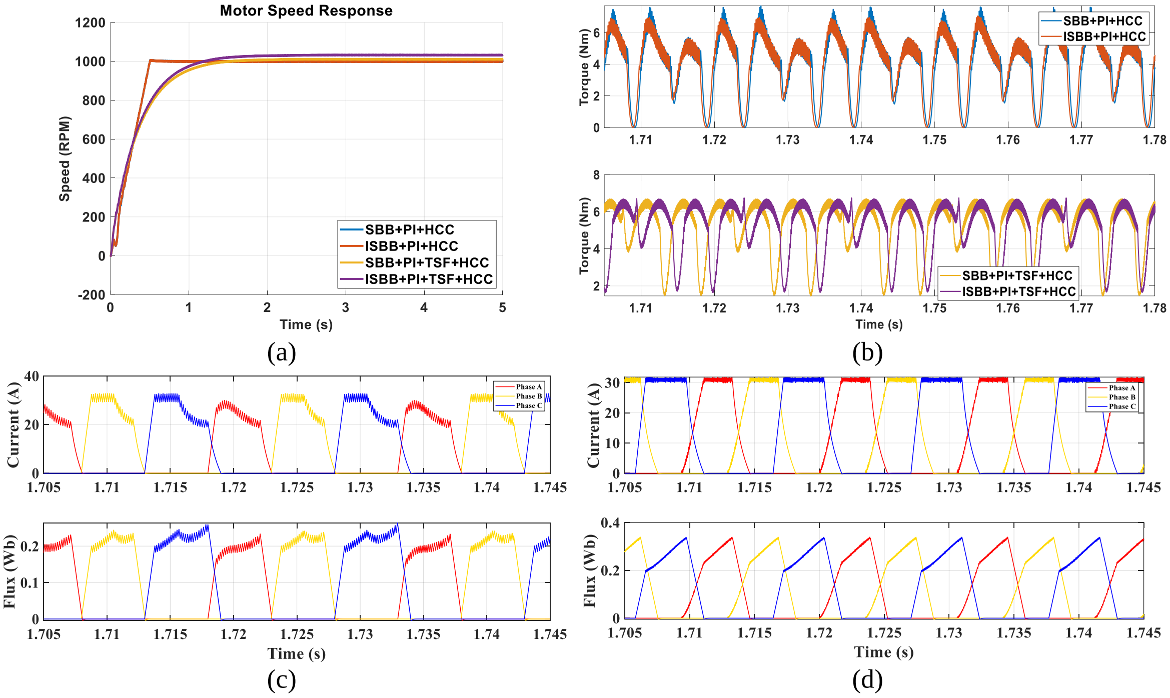

Figure 4. SRM parameters representation for case 1: (a) speed comparison of different control scheme for case 1, (b) Torque profile of different control scheme for case 1, (c) current and flux profile with PI and HCC for case 1, and (d) current and flux profile with PI, HCC and Improvised TSF for case 1

Table 1. Simulation results for TL = 2 Nm and reference speed of 1000 rpm

Control scheme	θ_{off}	k_p	K_i	Speed error (rpm)	Max torque (Nm)	Min torque (Nm)	THD
SBB with PI and HCC	79.78	4.10	35	0.06	6.93	0.007	0.47
ISBB with PI and HCC	79.46	3.24	33.87	0.05	6.97	0.004	0.45
SBB with PI, TSF, and HCC	78.3	3.15	29.5	0.05	7.04	0.005	0.257
ISBB with PI, TSF, and HCC	75.43	2.35	27.4	0.043	7.25	0.006	0.23
WOA with PI, TSF, and HCC	78.80	3.93	27.75	0.4	6.64	1.69	0.25
ACO with PI, TSF, and HCC	78.76	3.1	20.75	1.117	6.60	1.68	0.25
GSO with PI, TSF, and HCC	78.55	4.09	38.72	7.32	6.603	1.62	0.26
GA with PI, TSF, and HCC	78.65	4.9	11.03	6.62	6.56	1.65	0.26
PSO with PI, TSF, and HCC	78.8	3	31.11	3.02	6.64	1.73	0.25

3.2. Case 2

SRM is tested for TL=2 Nm and reference speed of 1500 rpm. Table 2 represents the simulation results of all the four control strategies for case 2. When the SRM is tested for case 2, the control scheme

SBB with PI and HCC resulted torque ripple of 1.51. For the control scheme, ISBB with PI, TSF and HCC, the torque ripple of 1.49. Figure 5(a) represents the speed comparison plot for all the four control schemes for case 2. Figure 5(b) represents the torque ripple comparison of four control schemes. In terms of torque ripple comparison, for the control scheme with PI and HCC, the ripples are sharp and uneven, but the control scheme with the implementation of TSF with adaptive sharing and small adaptive boosting, the torque ripples are less. Implementation of quintic polynomial and the usage of six boundary conditions have enhanced the speed regulation and torque profile.

Table 2. Simulation results for TL = 2 Nm and reference speed of 1500 rpm

Control scheme	θ_{off}	k_p	K_i	Speed error (rpm)	Max torque (Nm)	Min torque (Nm)	THD
SBB with PI and HCC	79.04	4.44	39.18	3	8.18	0.006	0.38
ISBB with PI and HCC	79.03	4.71	35.79	1	8.3	0.006	0.38
SBB with PI, TSF, and HCC	79.02	3	40	2	8.45	0.005	0.28
ISBB with PI, TSF, and HCC	78.86	4.5	31.3	0.05	8.75	0.004	0.29
WOA with PI, TSF, and HCC	78.65	4.46	40	2.25	8.49	2.79	0.27
ACO with PI, TSF, and HCC	78.85	4.7	21.73	9.41	8.49	2.93	0.23
GSO with PI, TSF, and HCC	78.86	3.9	37.8	9.65	8.49	2.93	0.23
GA with PI, TSF, and HCC	78.16	3.58	15.94	93.30	9.009	2.84	0.25
PSO with PI, TSF, and HCC	76.43	4.75	35.04	14	9.01	2.16	0.30

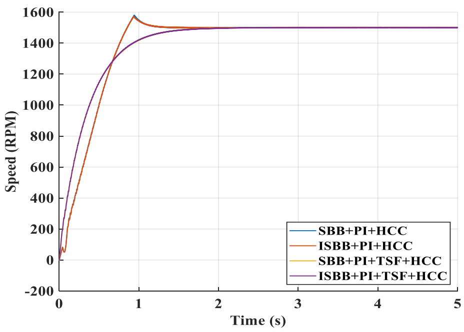

(a)

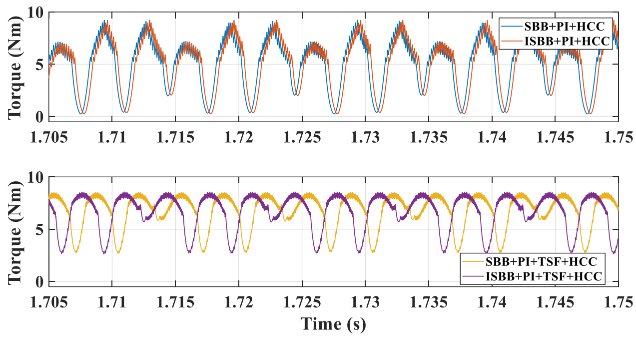

(b)

Figure 5. SRM parameters representation for case 2: (a) speed response of different control scheme for case 2 and (b) torque profile of different control scheme for case 2

3.3. Case 3

The simulation of SRM model is carried out for load torque of 3 Nm and reference speed of 1500 rpm. Table 3 represents the simulation values of case 3, TL = 3 Nm and reference speed 1500 rpm. With the increase in the load torque and reference speed, the maximum torque value has been increased for all the control schemes. Figure 6(a) represents the comparison of speed for all the four schemes. Figure 6(b) represents the torque ripple comparison of control schemes for PI with HCC and PI with TSF and HCC. For the control scheme, SBB with PI and HCC, the torque ripple is 1.53, for the control scheme ISBB with PI and HCC the torque ripple is 1.52. The torque ripple for control scheme with TSF is 0.89 and 0.88 for SBB and ISBB, respectively. For case 3, the improvised TSF is effective in improving the torque profile hence forth the torque profile.

Table 3. Simulation results for TL = 3 Nm and reference speed of 1500 rpm

Control scheme	θ_{off}	k_p	K_i	Speed error (rpm)	Max torque (Nm)	Min torque (Nm)	THD
SBB with PI and HCC	79.9	4.9	18.24	0.042	9.89	0.49	0.45
ISBB with PI and HCC	79.23	4.2	28	0.040	9.87	0.5	0.44
SBB with PI, TSF, and HCC	78.45	4.69	29.99	0.003	9.8	3.014	0.25
ISBB with PI, TSF, and HCC	78.45	3.65	22.28	0.002	9.85	3.106	0.24
WOA with PI, TSF, and HCC	80	4.24	40	7.53	9.6	3.68	0.20
ACO with PI, TSF, and HCC	79.74	3.86	16.01	3.26	9.6	3.55	0.21
GSO with PI, TSF, and HCC	79.66	4.6	11.81	10.43	9.6	3.48	0.21
GA with PI, TSF, and HCC	79.40	3	36.51	0.48	9.68	3.46	0.22
PSO with PI, TSF, and HCC	79.96	5	40	18	9.68	3.68	0.21

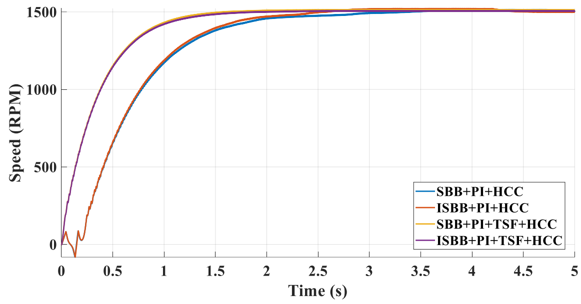

(a)

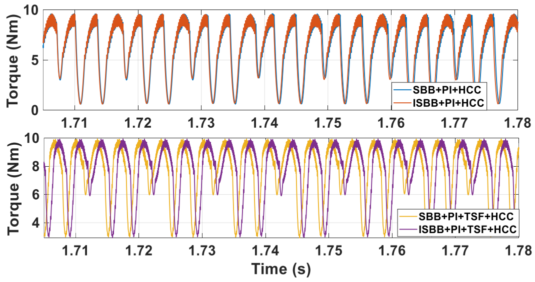

(b)

Figure 6. SRM parameters representation for case 3: (a) speed response of different control scheme for case 3 and (b) torque profile of different control scheme for case 3

3.4. Case 4

The SRM model is tested for load torque of 3 Nm and reference speed of 1000 rpm. Table 4 represents the simulation results of case 4. The SBB and ISBB algorithms compute the turn off angle and gain values for the PI controller based on the load torque on the reference speed values. For the control scheme, SBB with PI and HCC, the THD is 0.47 and the torque ripple is 1.64. For the control scheme, ISBB with PI and HCC, the THD is 0.46 and the torque ripple is 1.56. Figure 7(a) represents the speed plot for all the four schemes of case 4. Figure 7(b) represents the torque profile for all the four schemes of case 4. Figure 7(c) represents the current and flux profile for the control scheme of TSF with PI and HCC. Figure 7(d) represents the current and flux profile for the control scheme with PI and HCC. The torque ripple for control scheme with improvised TSF is 0.96 and 0.94 for SBB and ISBB implemented control scheme. Adaptive TSF is effective in enhancing the torque profile as compared with the PI and HCC control scheme The systems parameters for the proposed work are, stator poles = 6, rotor poles = 6, stator resistance = 0.012-ohm, inertia = 0.01 kg.m.m, friction= 0.03 N.m.s.

The control scheme consisting of improved TSF and ISBB is used for comparing with the existing algorithm. The iteration count considered is 10 with population size of 10. All the algorithms are tested for these iteration and population size. As per the results tabulated in Table 1, proposed ISBB performs better compared to the other algorithms. As per the results tabulated in Table 2, the ACO and GSO algorithms have computed better THD values, but the speed error recorded is considerably high. The proposed ISBB has demonstrated the balance in providing minimum error and acceptable THD. As per the results computed in Table 3, the algorithms GSO, WOA, ACO, GA, and PSO have computed better THD but with significant speed errors. ISBB has demonstrated reasonably minimum THD with the least speed error as compared to other algorithms. As per the results stated in Table 4, ISBB has demonstrated better results of THD and speed error as compared to other algorithms. Figures 8(a) and 8(b) represent the speed comparison graphs for TL = 3, 1500 rpm, and TL = 2 1500 rpm, respectively. The comparative analysis all the algorithms discussed in the proposed work is represented in Table 7. The proposed ISBB and TSF are implemented to compute the T_r and T_s.

Based on the rotor position and commutation, SRMs phase inductance changes, perfect timing must be maintained when the current is switching from one phase to another phase. With the knowledge of rising and settling time of torque, ensure the incoming phase generates positive torque before the outgoing phase enters the negative torque region. The work stated in [36], explains the importance of Modulation in current waveform leads to reduction in the torque ripples of the SRM.

Table 4. Simulation results for TL = 3 Nm and reference speed of 1000 rpm

Control scheme	θ_{off}	k_p	K_i	Speed error (rpm)	Max torque (Nm)	Min torque (Nm)	THD
SBB with PI and HCC	78.29	4.38	18.38	0.012	8.455	0.049	0.45
ISBB with PI and HCC	79.23	4.9	39.9	0.012	8.455	0.049	0.44
SBB with PI, TSF, and HCC	78.45	3.56	19	0.004	8.44	2.42	0.25
ISBB with PI, TSF, and HCC	78.45	3.65	17.31	0.002	8.85	2.56	0.24
WOA with PI, TSF, and HCC	78.58	4.2	38.93	2.22	7.84	1.99	0.26
ACO with PI, TSF, and HCC	78.54	3.66	31.7	1.01	7.85	1.95	0.26
GSO with PI, TSF, and HCC	78.21	4.65	20.14	1.33	7.93	1.86	0.28
GA with PI, TSF, and HCC	78.22	4.18	20.65	1.68	7.93	1.86	0.27
PSO with PI, TSF, and HCC	78.21	4.2	78.21	1.19	7.93	1.86	0.27

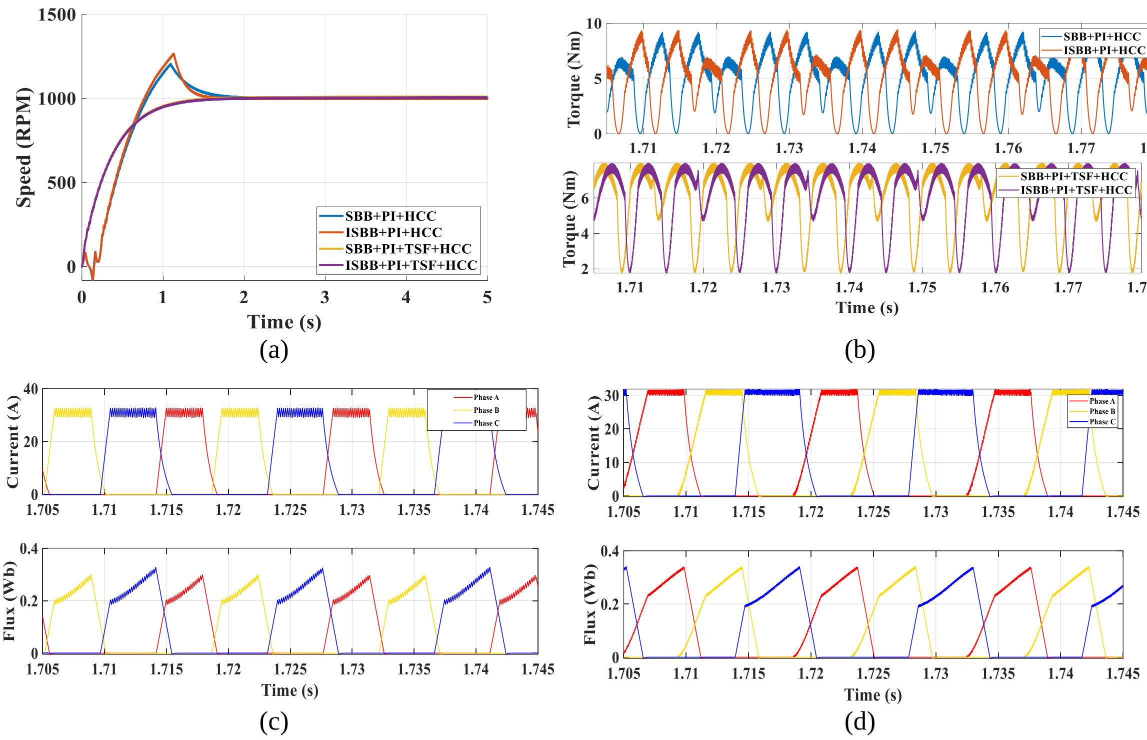

Figure 7. SRM parameters representation for case 4

Table 5 represents the torque rising and settling time for different reference speed and TL. The proposed ISBB has computed better Tr and Ts at all conditions, due to the enhanced feature of ISBB and improved TSF. Table 6 represents the simulation results for different firing angle demonstrating the robustness of ISBB. Table 7 represents the statistical performance analysis of ISBB and SBB under different reference speed and load torque condition. The SBB and ISBB was tested for 30 runs of simulation for each condition to compute the mean, variance standard deviation (STD) and confident interval. The tabulation of ISBB and SBB demonstrates the better performance of ISBB over SBB. Table 8 represents the comparative analysis of proposed ISBB with existing algorithms.

Table 5. Torque rising and settling time for different reference speed and TL

Parameter	Algorithm	1000 (rpm) TL = 2	1500 (rpm) TL = 3	1500 (rpm) TL = 2	1000 (rpm) TL = 3
T_r (sec)	ISBB	0.018	0.003	0.0021	0.002
	WOA	0.0017	0.0031	0.0021	0.0026
	ACO	0.0021	0.0034	0.0021	0.0027
	GSO	0.0015	0.0027	0.0027	0.0021
	GA	0.0026	0.0042	0.0026	0.0024
	PSO	0.0023	0.0025	0.0016	0.0027
T_s (sec)	ISBB	0.0022	0.0046	0.0021	0.0034
	WOA	0.0021	0.0038	0.0021	0.0032
	ACO	0.0024	0.0042	0.0026	0.0027
	GSO	0.0020	0.0035	0.0035	0.0028
	GA	0.0033	0.0051	0.0033	0.0030
	PSO	0.0028	0.0032	0.0021	0.0033

Table 6. Simulation results for different firing angle

θ_{on}	θ_{on}	Speed error (rpm)
42	75.82	0.05
43	76.31	0.01
44	70.40	0.01
46	78.60	0.01
47	71.006	0.01

Table 7. Statistical performance analysis of ISBB and SBB under different reference speed and load torque condition

Performance condition	Metrics	Mean		STD deviation		Variance		Confidence interval	
		ISBO	SBO	ISBO	SBO	ISBO	SBO	ISBO	SBO
TL=2, 1000 rpm	Speed error (rpm)	0.06	0.08	0.03	0.05	0.005	0.007	0.06±0.07	0.08±0.08
	Torque ripple (%)	0.06	0.075	0.08	0.066	0.006	0.056	0.06±0.09	0.075±0.09
	THD	0.27	0.46	0.003	0.045	0.00001	0.008	0.27±0.003	0.46±0.02
TL=2, 1500 rpm	Speed error (rpm)	0.05	0.07	0.04	0.048	0.0043	0.005	0.05±0.0086	0.07±0.02
	Torque ripple (%)	0.056	0.065	0.076	0.086	0.07	0.008	0.056±0.089	0.06±0.08
	THD	0.26	0.38	0.004	0.06	0.00001	0.0002	0.26±0.004	0.38±0.003
TL=3, 1000 rpm	Speed error (rpm)	0.045	0.060	0.053	0.72	0.288	0.0035	0.045±0.003	0.06±0.037
	Torque ripple (%)	0.07	0.057	0.002	0.0035	0.0006	0.0065	0.07±0.0023	0.05±0.08
	THD	0.23	0.38	0.0001	0.0020	0.00	0.001	0.23±0.007	0.38±0.04
TL=3, 1500 rpm	Speed error (rpm)	0.004	0.055	0.046	0.056	0.0037	0.0048	0.04±0.003	0.05±0.037
	Torque ripple (%)	0.065	0.07	0.002	0.0036	0.00	0.001	0.065±0.003	0.07±0.037
	THD	0.25	0.39	0.003	0.0056	0.00	0.0001	0.25±0.003	0.39±0.008

Table 8. Comparative analysis of proposed ISBB with existing algorithms

Algorithm	Advantage	Limitation
GA	Strong global search	Slower convergence
PSO	Fast convergence	Premature convergence
WOA	Better exploitation capability	Premature convergence
GSO	Good global search	Susceptible to local minimum
ACO	Effective combinatorial optimization	Can get stuck in local minimum
ISBB	Adaptive and stable	Simulation stage

3.5. Comparison with other existing methods

The proposed work is compared with other existing works as shown in Table 9. It is observed that proposed method provides the best results in terms of angle computation, gain value computation, torque profile and control response. Convergence graph is plotted for best fitness and iteration value for both SBB and ISBB. Figure 8(a) represents the convergence graph for the condition TL = 3 and reference speed of 1000 rpm. Figure 8(b) represents the convergence graph for the condition TL = 3 and reference speed 1500 rpm. Figure 8(c) represents the convergence graph for the condition TL = 2, 1500 rpm. Figure 8(d) represents the convergence graph for the condition TL = 2, 1000 rpm. Figure 9(a) and 9(b) speed error comparison at reference speed 1500 rpm and 1000 rpm, respectively. Figures 10(a) and 10(b) represents the comparison graph of Tr and Ts respectively at TL = 2 Nm and reference speed of 1000 rpm.

Table 9. Comparison of proposed methods with existing methods

Parameters	Proposed	Reference [37]	Reference [38]	Reference [39]	Reference [40]	Reference [41]	Reference [42]	Reference [43]
Angle computation	Adaptively	Adaptively	Adaptively	Adaptively	Manual	Manual	Adaptively	Adaptively
Gain values computation	Adaptively	-	-	-	-	-	-	-
Torque profile	Torque ripple: low	ripple: low	ripple: medium	Average torque attained is low, ripple: low	Initial overshoot in torque profile	Overshoot in torque ripple	Torque ripple: medium	Torque ripple: medium
Control response	Fast	Fast	Fast	Fast	Fast	Minor overshoot in initial speed	Fast	Fast

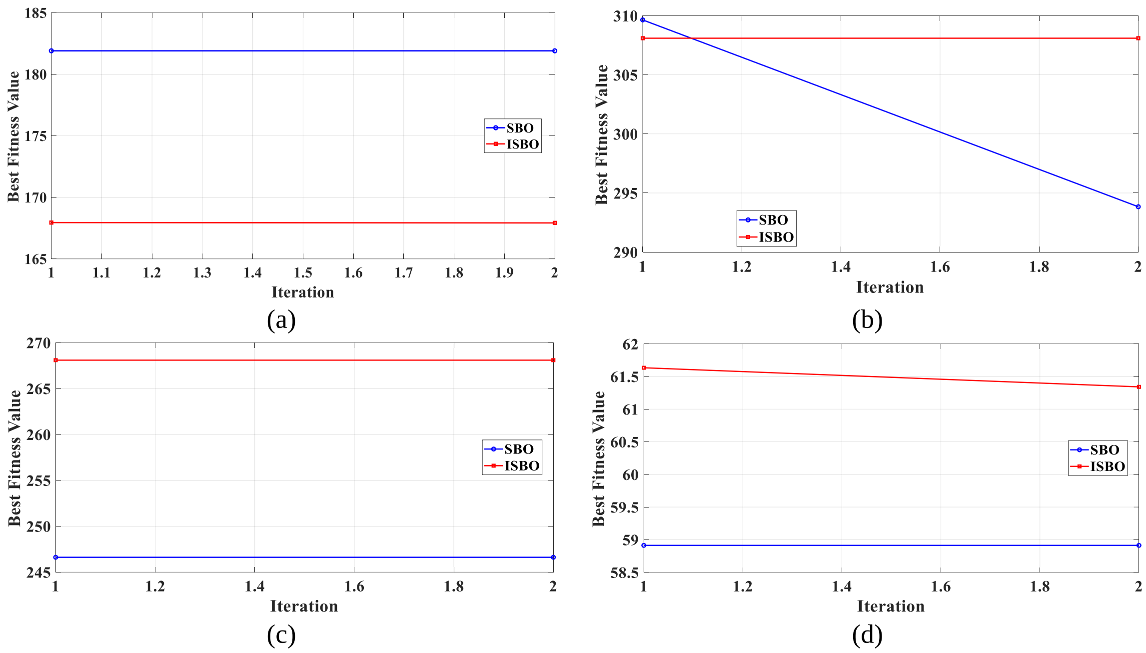

Figure 8. Convergence graph for different load torque and reference speed conditions

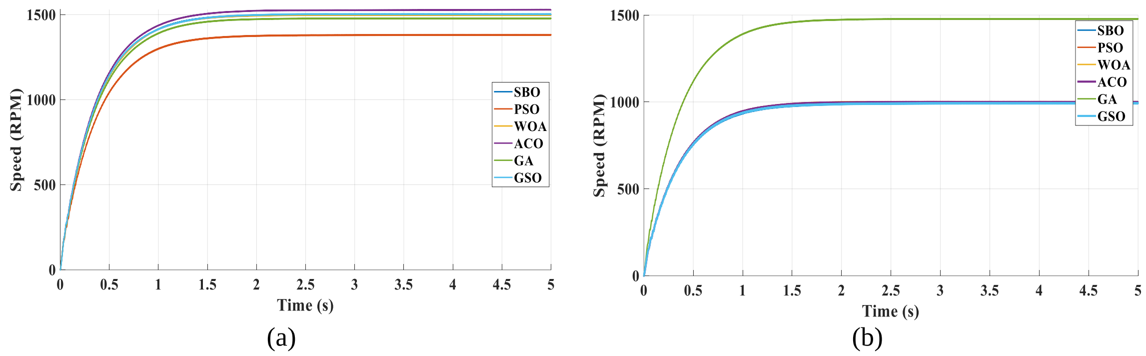

Figure 9. Speed error comparison at different reference speeds

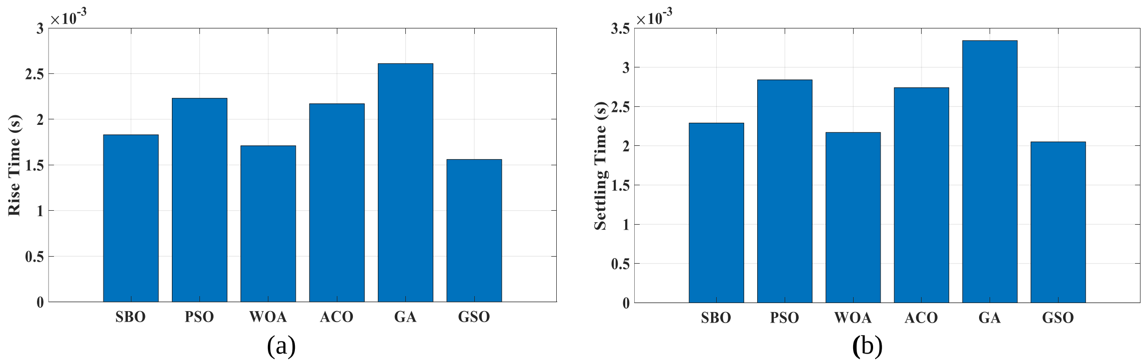

Figure 10. Comparison graph for T_r and T_s

4. CONCLUSION

In this work, a 6/4 SRM is considered. Two control schemes have been designed and implemented. The first control scheme consists of PI and HCC, and the second control scheme consists of PI with HCC and improvised TSF. ISBB is proposed and implemented to validate the performance of SRM under the two control schemes. The proposed work compares the performance of SRM drive for different control schemes namely, SBB with PI and HCC, ISBB with PI and HCC, SBB with PI, TSF and HCC and ISBB with PI, TSF, and HCC. The ISBB leads to better performance of SRM drive as it determines the best θ_{off}, k_p, K_i, T_r, and T_s to regulate speed and improve the torque profile. The performance of ISBB has been compared with the existing algorithms, the ISBB has provided the best trade in computing the parameters for SRM. The robustness of the ISBB is tested for different firing angle, which resulted in less speed error by computing better turn off angle. PI controllers are underrated but with the implementation of appropriate control scheme and metaheuristic algorithm such as ISBB, it can perform better. Currently, the work is limited to simulation validation, conforming the robustness of improvised TSF and ISBB. As a part of continued work, real time implementation confirms the robustness of improvised TSF and ISBB leading to enhanced performance of SRM. For all the four cases considered, the control scheme of ISBB with PI, TSF, and HCC has resulted in 50% reduction in THD as compared to conventional SBB with PI and HCC. It is evident that TSF majorly contributes to the reduction of THD and improving the torque profile of SRM by demonstrating lower T_r and T_s. The reduced torque and less T_r and T_s makes it suitable for energy efficient and high-performance drive applications. This shows the suitability of PI controllers with improved TSF and HCC along with the ISBB for speed regulation and torque ripple minimization for SRM drive.

ACKNOWLEDGMENTS

We sincerely thank Vidyavardhaka College of Engineering for encouraging to do the proposed research work.

FUNDING INFORMATION

Authors state no funding involved.

AUTHOR CONTRIBUTIONS STATEMENT

This journal uses the Contributor Roles Taxonomy (CRediT) to recognize individual author contributions, reduce authorship disputes, and facilitate collaboration.

Name of Author	C	M	So	Va	Fo	I	R	D	O	E	Vi	Su	P	Fu
M. Upanya	✓	✓	✓	✓	✓	✓		✓	✓	✓				
S. Rashmi	✓	✓			✓	✓			✓	✓	✓	✓	✓	

C : **C**onceptualization
M : **M**ethodology
So : **So**ftware
Va : **Va**lidation
Fo : **Fo**rmal analysis
I : **I**nvestigation
R : **R**esources
D : **D**ata Curation
O : Writing - **O**riginal Draft
E : Writing - Review & **E**diting
Vi : **Vi**sualization
Su : **Su**pervision
P : **P**roject administration
Fu : **Fu**nding acquisition

CONFLICT OF INTEREST STATEMENT

Authors state no conflict of interest.

DATA AVAILABILITY

The data that supports the findings of this study are available from the corresponding author, [MU], upon reasonable request.

REFERENCES

[1] B. Bilgin *et al.*, "Making the case for switched reluctance motors for propulsion applications," *IEEE Transactions on Vehicular Technology*, vol. 69, no. 7, pp. 7172–7186, Jul. 2020, doi: 10.1109/TVT.2020.2993725.

[2] N. A. Shibli and M. A. Mueller, "Design and optimization of low-speed, high-torque switched reluctance machines for wind energy applissscations: modeling techinques," in *2024 1st International Conference on Innovative Engineering Sciences and Technological Research (ICIESTR)*, IEEE, May 2024, pp. 1–6, doi: 10.1109/ICIESTR60916.2024.10798187.

[3] P. B. Sree and N. P. G. Bhavani, "Efficiency improvement of electrical vehicles using novel switched reluctance motor and compared with permanent magnet motor by reducing power loss," in *2023 6th International Conference on Contemporary Computing and Informatics (IC3I)*, IEEE, Sep. 2023, pp. 1473–1477, doi: 10.1109/IC3I59117.2023.10398050.

[4] B. H. Kumar, P. K. K. Reddy, N. R. Naik, M. Tharun, K. Nagaraj, and N. M. Babu, "Control of modified switched reluctance motor for EV applications," in *2022 Trends in Electrical, Electronics, Computer Engineering Conference (TEECCON)*, IEEE, May 2022, pp. 123–127, doi: 10.1109/TEECCON54414.2022.9854830.

[5] M. Sepehrinour, A. Kalantarikhalilabad, A. Rezaei-Zare, and A. Siadatan, "Optimal design, simulation, and sensitivity analysis of a C-shaped axial flux switched reluctance motor," in *2023 IEEE International Electric Machines & Drives Conference (IEMDC)*, IEEE, May 2023, pp. 1–7, doi: 10.1109/IEMDC55163.2023.10238855.

[6] S. S. Tata *et al.*, "Enhancing control strategy in switched reluctance motors (SRM): a focus on event-triggered control," in *2024 Control Instrumentation System Conference (CISCON)*, IEEE, Aug. 2024, pp. 1–6, doi: 10.1109/CISCON62171.2024.10696419.

[7] L. A. Quraan, A. L. Saleh, and L. Szamel, "Indirect instantaneous torque control for switched reluctance motor based on improved torque sharing function," *IEEE Access*, vol. 12, pp. 11810–11821, 2024, doi: 10.1109/ACCESS.2024.3355389.

[8] K. Diao, X. Sun, G. Bramerdorfer, G. Li, Q. Wang, and L. Wu, "A novel analytical design theory for switched reluctance motors incorporating nonlinear characteristics," *IEEE Transactions on Industrial Electronics*, vol. 72, no. 7, pp. 6775–6785, Jul. 2025, doi: 10.1109/TIE.2024.3511123.

[9] Z. Wang, X. Cao, Z. Deng, and J. Cai, "Electromagnetic modeling and investigation for bearingless switched reluctance motor considering magnetic saturation," *IEEE Transactions on Energy Conversion*, vol. 38, no. 1, pp. 122–133, Mar. 2023, doi: 10.1109/TEC.2022.3208831.

[10] G. Jegadeeswari, G. Ezhilarasi, V. Pramila, J. Vijayanand, and B. Kirubadurai, "Performance comparison of dynamic responses & speed control of switched reluctance motor using pi & fuzzy logic controller," in *2023 9th International Conference on Electrical Energy Systems (ICEES)*, IEEE, Mar. 2023, pp. 674–680, doi: 10.1109/ICEES57979.2023.10110237.

[11] S. Sontakke and S. Khubalkar, "Design of speed control scheme for switched reluctance motors in electric vehicles," in *2025 3rd World Conference on Communication & Computing (WCONF)*, IEEE, Jul. 2025, pp. 1–5, doi: 10.1109/WCONF64849.2025.11233532.

[12] R. K. Selvi and R. S. M. Malar, "A bridgeless Luo converter based speed control of switched reluctance motor using particle swarm optimization (PSO) tuned proportional integral (PI) controller," *Microprocessors and Microsystems*, vol. 75, p. 103039, Jun. 2020, doi: 10.1016/j.micpro.2020.103039.

[13] M. Rajakani, R. J. Kavitha, and S. Rajesh, "Feature selection using modified chaotic satin bowerbird algorithm with deep transfer learning for multispectral image classification," *International Journal of Information Technology*, vol. 17, no. 9, pp. 5549–5561, Dec. 2025, doi: 10.1007/s41870-024-01867-1.

[14] S. Mukhopadhyay, S. Sekaran, and S. Mansani, "Enhanced speed control of hybrid energy source-based switched reluctance motor employing PSO-tuned PI controller," in *2025 IEEE North-East India International Energy Conversion Conference and Exhibition (NE-IECCE)*, IEEE, Jul. 2025, pp. 1–6, doi: 10.1109/NE-IECCE64154.2025.11182735.

[15] B. Mirzaeian-Dehkordi and P. Moallem, "Genetic algorithm based optimal design of switching circuit parameters for a switched reluctance motor drive," in *2006 International Conference on Power Electronic, Drives and Energy Systems*, IEEE, Dec. 2006, pp. 1–6, doi: 10.1109/PEDES.2006.344356.

[16] N. Saha, S. Panda, and D. K. Sahoo, "Modified whale optimisation technique for combined objective of torque ripple minimization & speed control of SRM drive," in *2020 3rd International Conference on Energy, Power and Environment: Towards Clean Energy Technologies*, IEEE, Mar. 2021, pp. 1–5, doi: 10.1109/ICEPE50861.2021.9404396.

[17] N. Saha, S. Panda, and D. K. Sahoo, "Performance comparison of four phase SRM using many optimising Liaison and gravitational search algorithm," in *2018 International Conference on Applied Electromagnetics, Signal Processing and Communication (AESPC)*, IEEE, Oct. 2018, pp. 1–6, doi: 10.1109/AESPC44649.2018.9033247.

[18] A. Yildiz, M. Polat, and M. T. Ozdemir, "Design optimization of inverted switched reluctance motor using ant colony optimization algorithm," in *2018 International Conference on Artificial Intelligence and Data Processing (IDAP)*, IEEE, Sep. 2018, pp. 1–6, doi: 10.1109/IDAP.2018.8620923.

[19] M. W. Guo, J. S. Wang, L. F. Zhu, S. S. Guo, and W. Xie, "An Improved grey wolf optimizer based on tracking and seeking modes to solve function optimization problems," *IEEE Access*, vol. 8, pp. 69861–69893, 2020, doi: 10.1109/ACCESS.2020.2984321.

[20] F. Al-Amyal, L. Számel, and M. Hamouda, "An enhanced direct instantaneous torque control of switched reluctance motor drives using ant colony optimization," *Ain Shams Engineering Journal*, vol. 14, no. 5, p. 101967, May 2023, doi: 10.1016/j.asej.2022.101967.

[21] C. Huang, Y. Sun, J. Xu, and H. Li, "A novel direct instantaneous torque control strategy in permanent magnet-assisted switched reluctance motor based on optimization of conduction angle," *Alexandria Engineering Journal*, vol. 105, pp. 120–129, Oct. 2024, doi: 10.1016/j.aej.2024.06.089.

[22] P. Ren, J. Zhu, Z. Jing, Z. Guo, and A. Xu, "Improved DITC strategy of switched reluctance motor based on adaptive turn-on angle TSF," *Energy Reports*, vol. 8, pp. 1336–1343, Nov. 2022, doi: 10.1016/j.egyr.2022.08.076.

[23] M. Jabari and A. Rad, "Optimization of speed control and reduction of torque ripple in switched reluctance motors using metaheuristic algorithms based PID and FOPID controllers at the edge," *Tsinghua Science and Technology*, vol. 30, no. 4, pp. 1526–1538, Aug. 2025, doi: 10.26599/TST.2024.9010021.

[24] R. G. Intriago-Velasquez, J. P. C. Silveira, R. R. C. Castro, B. A. De Oliveira, T. A. dos S. Barros, and M. V. De Paula, "A modular H-bridge converter based SRM drive with integrated fault-tolerant capability for an agricultural hybrid vehicle," in *2025 Brazilian Power Electronics Conference (COBEP)*, IEEE, Oct. 2025, pp. 1–6, doi: 10.1109/COBEP66423.2025.11231513.

[25] L. Ge, J. Guo, C. Gong, G. Zhang, X. Ding, and S. Song, "Model predictive torque control of switched reluctance machines with torque sharing function and PWM control signals based on linear polynomial fitting," *IEEE Transactions on Power Electronics*, vol. 40, no. 1, pp. 40–45, Jan. 2025, doi: 10.1109/TPEL.2024.3444891.

[26] F. Jahangir *et al.*, "HGANet-23: a novel architecture for human gait analysis based on deep neural network and improved satin bowerbird optimization," *Signal, Image and Video Processing*, vol. 18, no. 8–9, pp. 5631–5645, Sep. 2024, doi: 10.1007/s11760-024-03260-8.

[27] S. Muthuselvan, S. Rajaprakash, R. Jaichandran, J. Antony, A. P. U, and I. V A, "Student academic performance prediction enhancement using t-SIDSBO and triple voter network," *Multimedia Tools and Applications*, vol. 83, no. 35, pp. 82223–82246, Mar. 2024, doi: 10.1007/s11042-023-17820-6.

[28] S. Suresh, J. Peter, and V. Chellappan, "Mathematical modeling and speed control of 6/4 switched reluctance motor drive," in *2022 International Conference on Futuristic Technologies in Control Systems & Renewable Energy (ICFCR)*, IEEE, Jul. 2022, pp. 1–6, doi: 10.1109/ICFCR54831.2022.9893644.

[29] C. Elmas and T. Yigit, "Genetic algorithm based on-line tuning of a PI controller for a switched reluctance motor drive," *Electric Power Components and Systems*, vol. 35, no. 6, pp. 675–691, Mar. 2007, doi: 10.1080/15325000601139674.

[30] S. A. Lakshmanan, B. S. Rajpurohit, and A. Jain, "Optimum setting algorithm based PI controller tuning for SRF-PLL used grid synchronization system," *Electric Power Components and Systems*, vol. 51, no. 6, pp. 538–554, Apr. 2023, doi: 10.1080/15325008.2023.2178544.

[31] S. Prajapati, R. Garg, and P. Mahajan, "Honey badger algorithm based PI controller for DC link voltage control of solar photovoltaic system connected to grid for enhanced power quality," *Electric Power Components and Systems*, vol. 53, no. 3, pp. 297–316, Feb. 2025, doi: 10.1080/15325008.2024.2304147.

[32] C. Huang, Y. Wu, H. Yuan, W. Cao, and Y. Geng, "An analytic method of segmented PWM duty cycle for switched reluctance motor," *CES Transactions on Electrical Machines and Systems*, vol. 7, no. 2, pp. 163–170, Jun. 2023, doi: 10.30941/CESTEMS.2023.00008.

[33] J. Liu, G. Wang, D. Liu, and Y. Fan, "An improved deadbeat control scheme for unipolar sinusoidal current excited switched reluctance motor drives," *IEEE Journal of Emerging and Selected Topics in Power Electronics*, vol. 11, no. 2, pp. 1589–1603, Apr. 2023, doi: 10.1109/JESTPE.2022.3222651.

[34] H. Lin, C. Cai, J. Chen, Y. Gao, S. Vazquez, and Y. Li, "Modulation and control independent dead-zone compensation for h-bridge converters: a simplified digital logic scheme," *IEEE Transactions on Industrial Electronics*, vol. 71, no. 11, pp. 15239–15244, Nov. 2024, doi: 10.1109/TIE.2024.3370975.

[35] O. B. Anderson, B. C. Barry, D. N. Hogan, and M. C. Duffy, "Hysteretic current mode control of a wide output voltage three-level converter," *IEEE Transactions on Power Electronics*, vol. 40, no. 5, pp. 6771–6786, May 2025, doi: 10.1109/TPEL.2024.3516518.

[36] R. F. Soliman, M. R. Ahmed, and S. M. Sharaf, "Torque ripples reduction of switched reluctance motor using direct torque control technique," in *2024 25th International Middle East Power System Conference (MEPCON)*, IEEE, Dec. 2024, pp. 1–6. doi: 10.1109/MEPCON63025.2024.10850288.

[37] Z. Touati and R. E. Araújo, "Speed control of switched reluctance motor with torque ripple reduction based on super-twisting sliding mode control," *IFAC-PapersOnLine*, vol. 59, no. 16, pp. 343–348, 2025, doi: 10.1016/j.ifacol.2025.10.127.

[38] S. Mukhopadhyay, S. Mansani, and S. Sekaran, "Torque ripple minimization and speed control of switched reluctance motor employing model predictive controller," *Electrical Engineering*, vol. 106, no. 6, pp. 7035–7054, Dec. 2024, doi: 10.1007/s00202-024-02425-5.

[39] M. Gengaraj and L. Kalaivani, "Mitigation of torque ripple in a switched reluctance motor using an interval type II fuzzy controller," *Automatika*, vol. 66, no. 4, pp. 1009–1026, Oct. 2025, doi: 10.1080/00051144.2025.2587941.

[40] A. L. Saleh, L. Számel, M. A. Abido, and M. Hamouda, "A novel reduced-ripple torque control technique for electric vehicle switched reluctance motors using an adaptive fuzzy neural network," *IEEE Open Journal of Power Electronics*, vol. 7, pp. 1133–1150, 2026, doi: 10.1109/OJPEL.2026.3678059.

[41] D. M, D. Samithas, P. K. Balachandran, and S. Selvarajan, "Experimental analysis of enhanced finite set model predictive control and direct torque control in SRM drives for torque ripple reduction," *Scientific Reports*, vol. 14, no. 1, p. 16805, Jul. 2024, doi: 10.1038/s41598-024-65202-1.

[42] M. Deepak and S. Devakirubakaran, "ANFIS-based SRM speed control and torque ripple mitigation for electric vehicle applications," *Soft Computing*, vol. 30, no. 4, pp. 2589–2608, Apr. 2026, doi: 10.1007/s00500-025-11013-z.

[43] F. P. Scalcon, G. Fang, C. J. V. Filho, S. Dhale, and B. Nahid-Mobarakeh, "Optimization of analytical TSFs for DC-link current reduction in switched reluctance motors," *IEEE Open Journal of Industry Applications*, vol. 5, pp. 356–368, 2024, doi: 10.1109/OJIA.2024.3441308.

BIOGRAPHIES OF AUTHORS

M. Upanya is an assistant professor in the Department of Electrical and Electronics Engineering at Vidyavardhaka College of Engineering, Mysuru, an autonomous institute affiliated with Visvesvaraya Technological University, Belagavi. She has five years of teaching experience and is currently pursuing her Ph.D. in the Department of Electrical and Electronics Engineering at Vidyavardhaka College of Engineering. She received her B.E. degree in electrical and electronics engineering from Cambridge Institute of Technology, Bengaluru, and her M.E. degree in control and instrumentation from Visvesvaraya College of Engineering, Bangalore University. Her research interests include power electronics, electrical machines, and motor drives. She can be contacted at email: upanya.m@vvce.ac.in.

S. Rashmi is an associate professor in the Department of Electrical and Electronics Engineering at Vidyavardhaka College of Engineering, Mysuru, an autonomous institute affiliated with Visvesvaraya Technological University, Belagavi. She received her Ph.D. degree in electronics from SJCE, Mysuru, her M.Tech. degree in VLSI design and embedded systems from SJCE, Mysuru, and her B.E. degree in electrical and electronics engineering from NIE, Mysuru. Her areas of interest include embedded systems, wireless sensor networks, VLSI, and materials science. She has 23 years of teaching experience. She can be contacted at email: rashmi.s@vvce.ac.in.